Kinetic Analysis of ^{18}F-Fluoride PET Images of Breast Cancer Bone Metastases

Robert K. Doot[1], Mark Muzi[1], Lanell M. Peterson[1], Erin K. Schubert[1], Julie R. Gralow[2], Jennifer M. Specht[2], and David A. Mankoff[1]

[1]Division of Nuclear Medicine, University of Washington and Seattle Cancer Care Alliance, Seattle, Washington; and [2]Division of Medical Oncology, University of Washington and Seattle Cancer Care Alliance, Seattle, Washington

The most common site of metastasis for breast cancer is bone. Quantitative ^{18}F-fluoride PET can estimate the kinetics of fluoride incorporation into bone as a measure of fluoride transport, bone formation, and turnover. The purpose of this analysis was to evaluate the accuracy and precision of ^{18}F-fluoride model parameter estimates for characterizing regional kinetics in metastases and normal bone in breast cancer patients. **Methods:** Twenty metastatic breast cancer patients underwent dynamic ^{18}F-fluoride PET. Mean activity concentrations were measured from serial blood samples and regions of interest placed over bone metastases, normal vertebrae, and cardiac blood pools. This study examined parameter identifiability, model sensitivity, error, and accuracy using parametric values from the patient cohort. **Results:** Representative time–activity curves and model parameter ranges were obtained from the patient cohort. Model behavior analyses of these data indicated ^{18}F-fluoride transport and flux (K_1 and Ki, respectively) into metastatic and normal osseous tissue could be independently estimated with a reasonable bias of 9% or less and reasonable precision (coefficients of variation $\leq$ 16%). Average ^{18}F-fluoride transport and flux into metastases from 20 patients (K_1 = 0.17 ± 0.08 mL·cm^{-3}·min^{-1} and Ki = 0.10 ± 0.05 mL·cm^{-3}·min^{-1}) were both significantly higher than for normal bone (K_1 = 0.09 ± 0.03 mL·cm^{-3}·min^{-1} and Ki = 0.05 ± 0.02 mL·cm^{-3}·min^{-1}, $P < 0.001$). **Conclusion:** Fluoride transport and flux can be accurately and independently estimated for bone metastases and normal vertebrae. Reasonable bias and precision for estimates of K_1 and Ki from simulations and significant differences in values from patient modeling results in metastases and normal bone suggest that ^{18}F-fluoride PET images may be useful for assessing changes in bone turnover in response to therapy. Future studies will examine the correlation of parameters to biologic features of bone metastases and to response to therapy.

Key Words: PET; ^{18}F-fluoride; radiotracer tissue kinetics; bone metastases; breast cancer

J Nucl Med 2010; 51:521–527
DOI: 10.2967/jnumed.109.070052

The most common site of metastasis for breast cancer is bone. Although bone scanning, CT, MRI, and other imaging modalities can readily detect skeletal metastases for breast cancer, bone metastasis response is currently difficult to assess in the clinic using these conventional modalities (*1,2*). Bone metastases from breast cancer present with a mixture of phenotypes ranging from osteoblastic to osteolytic lesions. One approach that may offer advantages for detecting, characterizing, and quantifying changes in bone metastases is the use of ^{18}F-fluoride PET (*2,3*).

Fluoride deposition accompanies the osteoblastic mineralization of new bony matrix by depositing fluoroapatite in place of the common bone mineral hydroxylapatite. The formation of fluoroapatite is favored over hydroxylapatite because the fluoroapatite crystal has less strain, a smaller unit cell size, less solubility, and a smaller specific surface area (*4*). The full skeletal kinetics of normal (*5*), osteoporotic (*6*) (including the precision of kinetic studies for osteoporotic women (*7*)), and Paget-diseased (*8*) bone have been studied using ^{18}F-fluoride PET.

Prior studies of fluoride kinetics have suggested that both parameters related to fluoride delivery (K_1) and incorporation into bone (Ki) may provide clinically useful information. K_1 has been shown to correlate to ^{15}O-H_2O-determined blood flow at low flow rates and follow the Renkin-Crone distribution at higher flow rates until reaching a maximum rate of about 0.2 mL·cm^{-3}·min^{-1} for ^{18}F-fluoride transport in porcine vertebrae (*9*). As such, K_1 may provide an indirect measure of bone metastasis blood flow that would be useful in assaying the effect of therapy on perfusion of metastases. Ki from dynamic scans of human vertebrae correlated with histomorphometric indices of bone formation rate from iliac crest bone biopsies collected within 4 mo of the PET scan ($P < 0.01$) (*10*). Ki from dynamic scans of porcine vertebrae were also found to correlate significantly with the mineral apposition rate ($P < 0.005$) from histomorphometry of iliac crest bone biopsies collected immediately before the PET scans (*11*). This property makes fluoride Ki an attractive parameter for assessing the effect of therapy on bone formation in bone with metastatic involvement.

The purpose of this analysis was to evaluate the ^{18}F-fluoride model for patients with breast cancer bone

Received Sep. 15, 2009; revision accepted Jan. 5, 2010.
For correspondence or reprints contact: Robert K. Doot, University of Washington, Box 357987, Seattle, WA 98195-7987.
E-mail: bdoot@uw.edu

metastases. We examined the sensitivity, precision, accuracy, and distribution of the ^{18}F-fluoride kinetic parameters in metastases and normal bone to identify parameters to consider as biomarkers in future serial PET studies seeking to quantify changes in bone at the site of metastasis in response to therapy.

MATERIALS AND METHODS

Patient Characteristics

Twenty patients with bone-dominant metastatic breast cancer underwent dynamic ^{18}F-fluoride PET before the start of new treatment. The patients signed informed consent for the PET studies according to the guidelines required by a Human Subjects Review Committee from the Institutional Review Board for the University of Washington/Fred Hutchinson Cancer Research Center.

PET

The ^{18}F-fluoride production, venous blood processing, PET acquisition, and image reconstruction protocols have been previously described (*12*). Only axial bone metastases and normal vertebrae were studied, to minimize the impact of lower-activity measurements due to the partial-volume effect of analyzing the typically smaller tumors and bone (*13*) located elsewhere.

Venous blood was sampled from 14 patients. Incomplete blood sampling from 1 patient because of equipment malfunction was censored. Directly measured blood time–activity curves were required only for patients whose blood pool was not in the PET field of view, resulting in 6 patients declining blood sampling.

Data Analysis

Data from the imaging studies were analyzed using a combination of PMOD 2.95 Build 5 (PMOD Technologies Ltd.), Excel, version 11.5.4 (Microsoft), Berkeley Madonna version 8.3.11 (Berkeley Madonna), and JMP 5.0 (SAS Institute) software packages.

Regions of Interest (ROIs). ROIs consisting of squares with 16 pixels and sides of 1.7 cm were drawn over the selected metastases, a normal vertebra, and the cardiac pool in the left ventricle if present in the imaging field of view. Tumor ROIs were placed on metastases with an osteoblastic component in dynamic scans using a separate reconstruction of summed data from the last 30 min of the ^{18}F-fluoride dynamic scan, whereas placement of ROIs for metastases that were primarily osteolytic required guidance from images from a contemporaneous clinical ^{18}F-FDG scan. Averages of the mean activity concentrations in ROIs drawn on 3 adjacent slices in each target volume were determined for each time point, taking care to avoid intervertebral disk spaces.

Model Input Function. A method for estimating an individual arterial ^{18}F-fluoride plasma clearance curve (*14*) was extrapolated to match our imaging time and scaled for individual patients based on 6 whole venous blood activity measurements from the last 30 min of imaging when venous blood activity was assumed equivalent to the arterial blood activity. Venous blood activities were measured from PET ROIs in the cardiac pool of 18 patients and from blood samples in 2 patients who did not have their heart in the field of view. The arterial plasma input function was calculated by multiplying the whole arterial blood input function by the average plasma–to–whole blood ratio of ^{18}F-fluoride concentrations of 1.2 ± 0.2 (±SD, n = 22) from 13 patients with complete venous blood and plasma activity measurements. Both population-based arterial input functions (plasma and whole blood) were used for kinetic modeling of fluoride uptake.

2-Compartment Kinetic Model. We used the 2-compartment model originally proposed by Hawkins et al. (*5*) consisting of a bone compartment with unbound ^{18}F-fluoride and another compartment with ^{18}F-fluoride bound to bone, with the changing concentration of ^{18}F-fluoride in blood plasma serving as the input function. Transfer of fluoride into the tissue (K_1), washout of unretained tissue fluoride to blood (k_2), incorporation of fluoride into bone (k_3), and release of incorporated fluoride (k_4) were 4 of 5 parameters estimated via nonlinear regression using PMOD software. On the basis of previous experience, a fifth parameter for the start of the blood input function was floated ±2 min to account for any delays between the start of the input function and the start of ^{18}F-fluoride delivery to the tumor. The macroparameter for the net flux of fluoride into bone, Ki, was calculated as shown in the following equation (*5*):

$$\text{Flux, Ki} = \frac{K_1 k_3}{k_2 + k_3}, \qquad \text{Eq. 1}$$

where Ki has units of mL·cm^{-3}·min^{-1}. The original parameter k_2 from the ^{18}F-fluoride model of Hawkins et al. (*5*) was replaced with K_1/k_2 to improve the approach to model fitting based on early identifiability analyses (data not shown). We report in place of the K_1/k_2 term the equivalent V_D, which is the volume of distribution of fluoride in tissue with units of mL·cm^{-3}.

The blood volume fraction in the imaged tissue was a potential sixth floating parameter for this model that was set constant to the mean floated value of 0.030 based on a study of porcine vertebrae (*11*). Early analysis suggested that both the blood volume fraction and K_1 could not be independently estimated so the blood volume fraction was set to a reasonable physiologic value to allow an independent estimation of K_1, which was expected to be more important in evaluating changes in bone physiology due to therapeutic response. The starting parameter values of 0.1 mL·cm^{-3}·min^{-1}, 0.5 mL·cm^{-3}, 0.1 min^{-1}, and 0.01 min^{-1} for K_1, V_D, k_3, and k_4, respectively, were derived from average estimates from a study of ^{18}F-fluoride uptake in vertebrae of 72 postmenopausal women (*6*).

Parameter range constraints for estimations of K_1, V_D, k_3, and k_4 were 0.001–1.0 mL·cm^{-3}·min^{-1}, 0.05–10 mL·cm^{-3}, 0.001–1.0 min^{-1}, and 0.0001–0.5 min^{-1}, respectively. Near zero, lower bounds could occur when studying necrotic or fibrotic tissue. On the basis of initial analysis of the data, the maximum value for K_1 estimates was 5-fold the approximate maximum value of 0.2 mL·cm^{-3}·min^{-1} for K_1 estimated from porcine ^{18}F-fluoride and ^{15}O-H_2O studies (*9*). Because chloride membrane transporters use active transport to achieve intracellular concentrations of chloride that are 4-fold higher than expected by passive diffusion (*15*), maximum V_D values for fluoride that use the same transporters for normal tissue should be less than 4. The maximum estimate for V_D was set to 10 mL·cm^{-3} to allow for metastases with aberrantly higher rates of fluoride influx and model expansion during nonlinear optimization. Estimates for k_3 were limited to 5-fold the average estimated k_3 value of 0.2 min^{-1} for 7 patients with vertebral Paget disease (*8*). The maximum estimate for k_4 was set to half of the maximum value for k_3 because k_4 was expected to always be less than k_3. Fluoride incorporation into bone is favored

because of the reduction in bone crystal strain, solubility, and specific surface area (*4*).

Model Characterization. After setting starting values and estimation ranges for the proposed model, it was characterized with respect to parameter sensitivity, identifiability, and susceptibility to noise to identify which kinetic parameters may be useful for evaluating changes in bone physiology due to response to therapy. We used our previously published methods (*16–19*), summarized in the following paragraphs.

Sensitivity functions for model parameters were calculated by determining the change in model output resulting from a 1% deviation in the individual parameter. The identifiability of the individual parameters was assessed from a correlation matrix generated using the average blood input function and tissue time–activity curves for bone metastases and normal vertebrae from a subset of 11 patients for whom we had complete sets of blood time–activity curves from blood sampling and cardiac blood-pool ROIs (*16*).

Precisions of model estimates of K_1, V_D, k_3, k_4, and the flux macroparameter Ki were calculated using a Monte Carlo technique and simulated tissue time–activity curves that had 2% Poisson noise (based on typical patient imaging noise) added 250 times to 1 typical metastasis and 1 normal bone tissue uptake curve. Parameter estimates were compared with original parameters to determine the parameter coefficients of variation (COVs) and biases (*16*).

Unlike Monte Carlo precision analyses that repeatedly added noise to just 1 time–activity curve per tissue type, accuracies of parameter estimations were better evaluated by adding 2% Poisson noise to 250 different original time–activity curves for both osseous tissue types. The original time–activity curves were generated from a range of randomly selected parameter values inside the expected ranges for tumor and normal bone for our patient population. The original and estimated parameter values were compared by calculating their correlation coefficient, determining percentage bias between original and estimated values, and calculating the estimation precision by dividing the SEE for the estimated regressed against the original parameter plots by the mean original parameter (SEE/mean) (*16*).

Analysis of Patient Results. Metastases analyzed from fluoride PET scans were characterized as lytic or sclerotic on the basis of a review of contemporaneous CT scans available for 19 of 20 patients. Lesions that were predominantly less radiographically dense than surrounding bone were considered lytic, whereas lesions that were denser than surrounding bone were classified as sclerotic. The model was then applied to patient PET studies to estimate the parameter distributions and compare their mean values for metastatic and normal bone and lytic and sclerotic lesions. Distributions of estimates for K_1, V_D, k_3, k_4, and calculated flux (Ki) for both metastases and normal bone were shown using quantile box plots. Because fluoride Ki and K_1 are measurements of different physiologic functions, we used different correlation coefficients, different values of the SE estimate divided by the mean (SEE/mean), and differences in the squared residuals to compare plots of Ki versus K_1 for bone metastases in the axial skeleton and normal vertebrae to examine variability in their relationship. Differences between parameter values for lytic and sclerotic lesions were examined using 2-sided P values from Wilcoxon rank-sum tests. Paired differences between parameter values and differences between squared residuals of plots of Ki versus K_1 for metastatic and normal bone tissue were examined using 2-sided P values from Wilcoxon signed rank tests. Statistical analyses of clinical patient results were conducted using JMP 5.0. P values less than 0.05 were considered significant.

RESULTS

Patient Characteristics

Twenty breast cancer patients with bone-dominant metastatic breast cancer with an axial bone metastasis in the field of view underwent dynamic ^{18}F-fluoride PET before the start of new treatment. Most patients were actively being treated for metastatic disease, with some evidence of progressive disease that prompted a change in therapy; a few patients were therapy-naïve. Seventeen patients had received no new chemotherapy or hormone or radiation therapy for the 3 mo before their PET scan. Two patients with sclerotic lesions at the time of the fluoride PET study had started a new chemotherapy regime, and 1 patient with a lytic lesion started hormone therapy less than 3 mo before their PET scans. Phenotypes of examined bone metastases were classified from available contemporaneous CT scans as 11 lytic and 8 sclerotic lesions, with an average long dimension of 28 ± 8 mm and a minimum long dimension of 15 mm. Representative fluoride and ^{18}F-FDG PET images for a patient with a sclerotic metastasis and a patient with a lytic metastasis are shown in Figure 1. The mean patient age was 52 y (range, 34–78 y). The mean injected dose was 3.6 MBq/kg (range, 2.8–4.5 MBq/kg).

Model Behavior

The sensitivity functions for each parameter were plotted versus time in Figure 2 and were similar for both bone metastases and normal vertebrae. The model was selectively sensitive to K_1 during early imaging time bins when

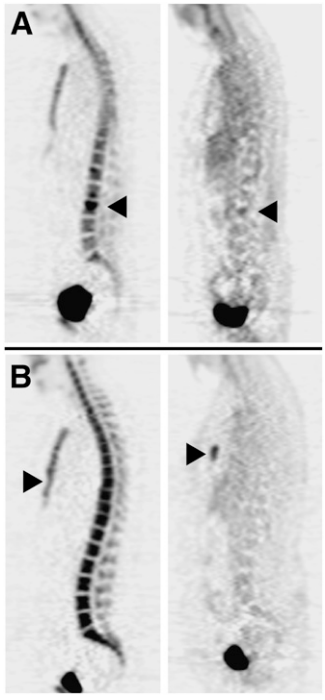

FIGURE 1. Sagittal ^{18}F-fluoride images (left) and ^{18}F-FDG images (right) for 2 patients exhibiting bone-dominant breast cancer metastases (arrowheads). (A) First patient (top) has primarily sclerotic tumor that is clearly visible in ^{18}F-fluoride image. (B) Second patient (bottom) has lytic tumor that is evident as photopenic region in ^{18}F-fluoride image and enhanced region in ^{18}F-FDG image.

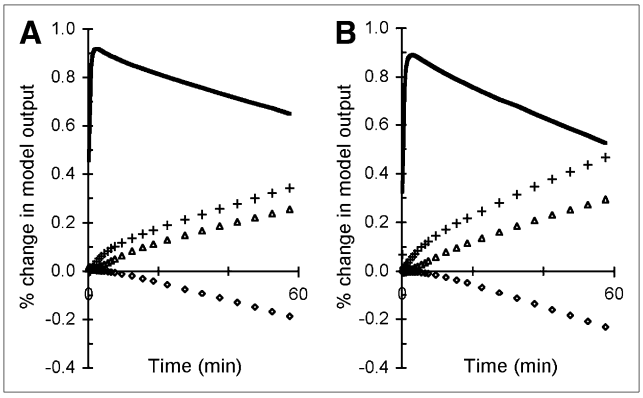

FIGURE 2. Sensitivity functions representing time-dependent percentage change in model output resulting from ±1% change in parameters K_1 (solid line), V_D (crosses), k_3 (△), and k_4 (◇) are shown for axial breast cancer bone metastases (A) and normal bone vertebrae (B).

the model was relatively insensitive to the other floated parameters, indicating that independent measurements of K_1 were feasible. The sensitivity functions (Fig. 2) indicate V_D, k_3, and k_4 parameters may be difficult to estimate independently because the model was most sensitive to all these parameters at the same time. The correlation coefficients between K_1 and k_4 estimates for metastases and normal bone (Table 1) have relatively low absolute values, suggesting that independent measurement of k_4 may be possible.

Precision-simulated estimates of parameter COVs and biases using the Monte Carlo approach (Table 2) were initiated using average parameter estimates from 20 patients for K_1, V_D, k_3, and k_4 listed in the table as the original value for the simulated curves. The 2 original flux values (Ki) in Table 2 were calculated using the corresponding 4 original parameter values for each tissue type. The magnitudes of the predicted COVs for estimates of V_D, k_3, and k_4 were large and ranged from 38% to 87%. The relatively low

TABLE 1. Covariance Matrices for Bone-Dominant Metastatic Breast Cancer and Normal Vertebrae

Parameter	K_1*	V_D†	k_3‡	k_4‡
Axial bone metastases				
K_1	1	—	—	—
V_D	−0.82	1	—	—
K_3	0.65	−0.96	1	—
K_4	−0.38	−0.14	0.39	1
Normal vertebrae				
K_1	1	—	—	—
V_D	−0.90	1	—	—
K_3	0.79	−0.97	1	—
k_4	0.09	−0.44	0.64	1

*mL·cm^{-3}·min^{-1}.
†mL·cm^{-3}.
‡min^{-1}.

TABLE 2. Parameter Biases and Errors from Monte Carlo Analyses

Parameter	Original value	Mean estimate	Bias	COV
Axial bone metastases (n = 250)				
K_1*	0.166	0.177	7%	12%
V_D†	2.81	2.69	−4%	53%
K_3‡	0.288	0.401	39%	38%
K_4‡	0.052	0.064	23%	75%
Ki*	0.138	0.142	3%	4%
Normal vertebrae (n = 250)				
K_1*	0.091	0.099	9%	11%
V_D†	1.94	1.64	−16%	74%
K_3‡	0.165	0.338	105%	72%
K_4‡	0.067	0.068	2%	87%
Ki*	0.071	0.072	2%	16%

*mL·cm^{-3}·min^{-1}.
†mL·cm^{-3}.
‡min^{-1}.

absolute levels of bias and COV for K_1 (≤9% and ≤12%) and for Ki (≤3% and ≤16%) suggested that robust model estimates for these 2 parameters in both metastases and normal bone are possible.

A previous study suggested that the estimation of k_4 in the 2-compartment model was unreliable and degraded precision in estimates of Ki (*7*). To test this approach, our Monte Carlo error analysis was repeated using a 3-parameter model in which k_4 was fixed to 0 min^{-1} during optimization (i.e., estimating only K_1, V_D, and k_3) to determine whether this would improve the precision of Ki estimates and to assess any resulting change in estimation biases. This was done for 2 sets of metastatic bone starting values: same original values as used for the results in Table 2 and repeated with k_4 originally set as 0.01 min^{-1}, which was a previously reported value for normal vertebrae (*6*). When the original starting value for k_4 was 0.05 min^{-1}, the modeling results showed higher absolute values of bias and COV for Ki when k_4 was fixed to zero (−32% and 6%) than when floated during optimization (Table 2, 3% and 4%). However, when the original starting value for k_4 was 0.01 min^{-1}, the biases and COVs in Ki estimates were similar when k_4 was fixed to zero (−2.1% and 1.5%) or floated during optimization (2.8% and 2.9%).

Estimated accuracies of parameter estimates by simulating over the clinical range of parameters for the axial bone metastases and normal vertebrae are shown in Figure 3 and summarized in Table 3. The magnitudes of the predicted SEE divided by the mean (SEE/mean) for estimates of V_D, k_3, and k_4 were large and ranged from 40% to 66%. Estimated versus the original values for K_1 and Ki were highly correlated (r = 0.96 and r = 0.99, respectively) and had corresponding low SEE/mean values of 13% and 9%.

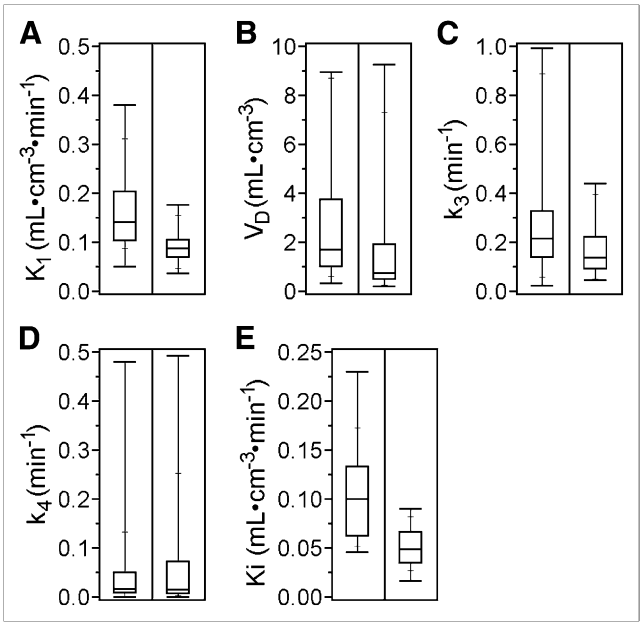

FIGURE 3. Quantile box plots of ^{18}F-fluoride modeling results for 20 patients with breast cancer bone metastases. Tumor results appear in left panels and normal bone in right panels for 4 floating model parameters (K_1 [A], V_D [B], k_3 [C], and k_4 [D]) and for flux macroparameter, Ki (E). Top, middle, and bottom box lines in plots represent 75th, 50th, and 25th percentiles, whereas extent of vertical lines shows range of parameter values.

Patient Modeling Results

The average, SD, and COV results from patient modeling are in Table 4, and the median and distribution results are in Figure 3. An example patient's ^{18}F-fluoride time–activity curves for the cardiac blood pool and a bone metastasis appear in Supplemental Figure 2 (supplemental materials are available online only at http://jnm.snmjournals.org), with the corresponding scaled whole-blood input function and model fit of the tumor time–activity curve. The average K_1 and Ki for lytic lesions (K_1 = 0.186 ± 0.098 mL·cm^{-3}·min^{-1} and Ki = 0.109 ± 0.057 mL·cm^{-3}·min^{-1}) were higher than for sclerotic lesions (K_1 = 0.135 ± 0.058 mL·cm^{-3}·min^{-1} and Ki = 0.086 ± 0.024 mL·cm^{-3}·min^{-1}). However, the differences between K_1, V_D, k_3, k_4, Ki, and Ki/K_1 for lytic and sclerotic metastases were not significant ($P \geq 0.10$). Only differences in model estimates of K_1 and Ki for bone metastases and normal vertebrae were significantly different ($P < 0.001$).

TABLE 3. Parameter Accuracy over Range of Values (n = 250)

Parameter	r*	Bias	SEE/mean†
K_1	0.96	1%	13%
V_D	0.58	−5%	40%
k_3	0.62	47%	58%
k_4	0.66	11%	66%
Ki	0.99	2%	9%

*Correlation coefficient.
†SEE/mean or SE estimate/mean is estimate of associated error.

TABLE 4. Parameter Modeling Results

Parameter	Mean estimate	SD	COV
Axial bone metastases (n = 20)			
K_1*	0.166†	0.084	50%
V_D‡	2.81	2.60	92%
K_3§	0.288	0.257	89%
K_4§	0.052	0.107	205%
Ki*	0.103†	0.048	47%
Ki/K_1	0.673	0.218	32%
Normal vertebrae (n = 20)			
K_1*	0.091†	0.035	38%
V_D‡	1.94	2.52	130%
K_3§	0.165	0.107	65%
K_4§	0.067	0.121	181%
Ki*	0.052†	0.020	38%
Ki/K_1	0.597	.202	34%

*mL·cm^{-3}·min^{-1}.
†Metastases K_1 and Ki values were significantly different from their normal values ($P < 0.001$).
‡mL·cm^{-3}.
§min^{-1}.

After determining that transport and flux were the only 2 model measures that could be accurately estimated with reasonable precision, we sought to characterize any relationship between the Ki and the K_1 values. The slopes and correlations of K_1 versus Ki (Fig. 4) were similar for both metastatic and normal bone (tumor slope = 0.27, r = 0.47; bone slope = 0.28, r = 0.49). The SEE for Ki, when regressed against K_1, divided by the mean value of Ki was higher for metastases (SEE/mean = 0.42) than for normal vertebrae (SEE/mean = 0.34). The variability in the relationship for Ki versus K_1 determined by the paired squared residuals was significantly higher for metastases (0.0017 ± 0.0029) than for normal bone (0.0003 ± 0.0003, P = 0.019), indicating, as expected, a greater variability in the relationship between parameters for metastases versus bone.

DISCUSSION

We used dynamic ^{18}F-fluoride PET to characterize fluoride kinetics of bone metastases in breast cancer patients. Our analyses included using model simulations to determine parameter identifiability and likely precision and accuracy as well as analyses of patient data from baseline dynamic ^{18}F-fluoride PET scans. We found that ^{18}F-fluoride transport (K_1) and flux (Ki) were significantly different in metastases and normal bone and could be estimated with reasonable precision and accuracy.

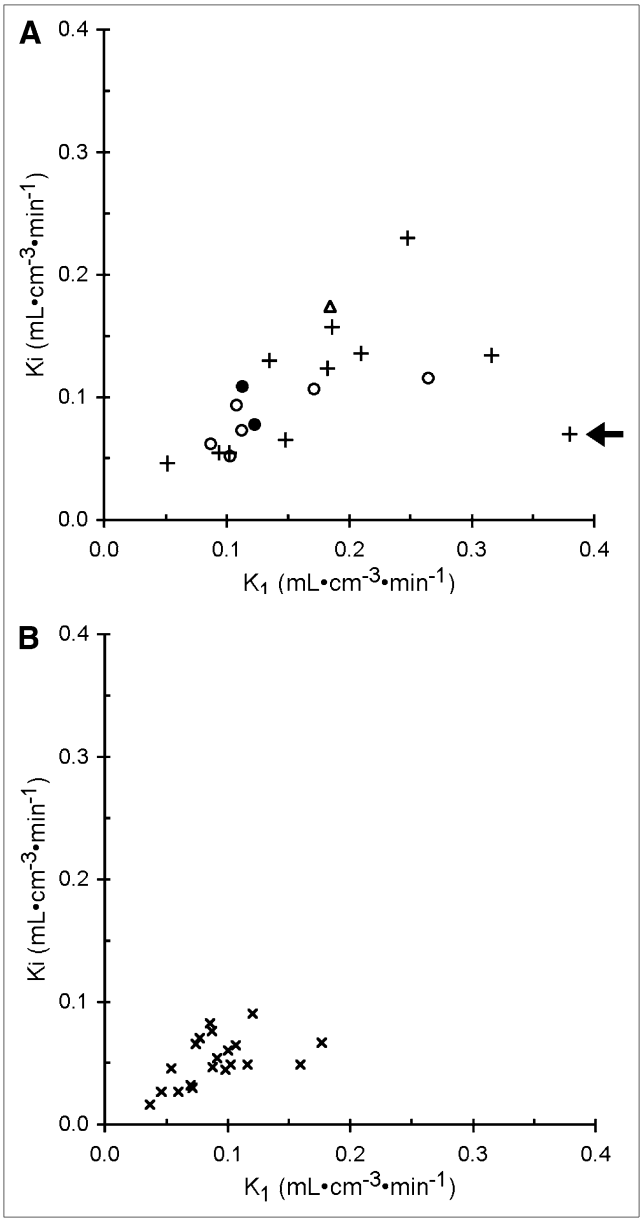

FIGURE 4. Model parameter correlation plots of ^{18}F-fluoride flux, Ki, vs. transport, K_1, for 20 axial breast cancer bone metastases classified from CT analysis to be either lytic (crosses), sclerotic (○), or unknown (△) (A) and normal bone vertebrae (B). Filled circles (●) identify 2 patients whose chemotherapy changed less than 3 mo before their PET scan. Arrow indicates lytic tumor identified in Figure 1B.

Low K_1 and Ki COV values (range, 4%−16%) from Monte Carlo simulations, low K_1 and Ki bias estimates no more than 2% from model accuracy simulations, and correlation coefficients of greater than or equal to 0.96 for plots of estimated versus original values of K_1 and Ki indicate the feasibility of using these PET measures to study both bone metastases and normal bone. The levels of bias (≤23%) and COV (≥75%) for k_4 in Table 2 indicate that only large changes in k_4 may be detectable, suggesting that changes in k_4 as a measure of bone lysis may not be feasible. Lower correlation coefficients ($r \leq 0.66$, Table 3) and a higher predicted range of COV from 38% to 87% (4-parameter model, Table 2) for estimates of V_D, k_3, and k_4 suggest that model estimates of these parameters will not be useful PET measures to assess bone cancer diagnosis and progression. It is possible that longer scanning times might improve the estimates of k_4, and possibly V_D and k_3; however, scanning for longer than 1 h is likely to be challenging for many patients with bone metastases.

Repeating the Monte Carlo analysis with $k_4 = 0$ min^{-1} as suggested by Frost et al. to increase the precision of fluoride Ki measures (*7*) resulted in a Ki bias estimate of −32% and decreased precision from 4% to 6% COV from when using the original values in Table 2 ($k_4 = 0.05$ min^{-1}). When Monte Carlo analyses were repeated with the original k_4 for metastases set to a reported normal value of 0.01 min^{-1} (*6*), the Ki bias and COV estimates resulting from a floated k_4 were similar to the estimates when $k_4 = 0$ min^{-1}. This result suggests that when estimating fluoride Ki for bony tissues that may have a strong osteolytic component, it is better to float k_4 than to risk an increase in the bias of Ki estimates by a factor of 10.

There was considerable phenotypic variability in the bone metastases that was reflected in the fluoride parameter estimates in individual patients. Our results suggest that fluoride delivery and flux into mineralized bone are not necessarily coupled for these metastases. The level of heterogeneity is not surprising considering our diverse patient population with differing treatment histories. The absence of significant differences between parameters for metastases classified as lytic or sclerotic by contemporaneous CT scans was not surprising considering most of the metastases appeared to have both lytic and sclerotic aspects (Fig. 1A). In addition, it is likely that prior treatment may have changed the apparent phenotype of the lytic lesions to a more sclerotic variety. This flare response has been described qualitatively for bone scintigraphy and fluoride PET (*2,20*) and will need to be considered in evaluating changes in response to treatment. The simulated precision of K_1 and Ki parameter estimates and the ability of dynamic ^{18}F-fluoride PET to quantify a significant difference between both fluoride delivery and flux into the metastases and normal bone suggest these PET scans may be useful for quantifying changes in bone metastasis physiology in response to therapy and helpful in understanding the effect of cancer therapies on bone lysis and new bone formation.

CONCLUSION

Simulations suggest both K_1 and Ki can reasonably quantify ^{18}F-fluoride kinetics in breast cancer bone metastases and normal bone because of low parameter biases (≤9%), high correlations between estimated and original values ($r \geq 0.96$), and low associated errors (COV ≤ 16%).

Both K_1 and Ki are promising for the evaluation of changes in bone physiology in response to therapy because values for metastases were significantly different from those for normal bone ($P < 0.001$). The ability to model both ^{18}F-fluoride transport (K_1) and ^{18}F-fluoride flux (Ki) with dynamic PET scans provides a robust method for measuring fluoride delivery and bone formation at the site of bone metastases and possibly for quantifying response to therapy, but more investigation is needed.

ACKNOWLEDGMENTS

We thank Dr. Brenda F. Kurland for discussion of statistics, University of Washington radiochemists for isotope production, and physicists and technicians for assistance with the imaging. We also acknowledge the referring oncologists and staff from the Seattle Cancer Care Alliance. This work was supported by grants CA124573, CA72064, and RR17229 from the National Institutes of Health.

REFERENCES

1. Hamaoka T, Madewell JE, Podoloff DA, Hortobagyi GN, Ueno NT. Bone imaging in metastatic breast cancer. *J Clin Oncol.* 2004;22:2942–2953.
2. Even-Sapir E. Imaging of malignant bone involvement by morphologic, scintigraphic, and hybrid modalities. *J Nucl Med.* 2005;46:1356–1367.
3. Petren-Mallmin M, Andreasson I, Ljunggren O, et al. Skeletal metastases from breast cancer: uptake of ^{18}F-fluoride measured with positron emission tomography in correlation with CT. *Skeletal Radiol.* 1998;27:72–76.
4. Grynpas MD. Fluoride effects on bone crystals. *J Bone Miner Res.* 1990;5(suppl 1):S169–S175.
5. Hawkins RA, Choi Y, Huang SC, et al. Evaluation of the skeletal kinetics of fluorine-18-fluoride ion with PET. *J Nucl Med.* 1992;33:633–642.
6. Frost ML, Fogelman I, Blake GM, Marsden PK, Cook G Jr. Dissociation between global markers of bone formation and direct measurement of spinal bone formation in osteoporosis. *J Bone Miner Res.* 2004;19:1797–1804.
7. Frost ML, Blake GM, Park-Holohan SJ, et al. Long-term precision of ^{18}F-fluoride PET skeletal kinetic studies in the assessment of bone metabolism. *J Nucl Med.* 2008;49:700–707.
8. Cook GJ, Blake GM, Marsden PK, Cronin B, Fogelman I. Quantification of skeletal kinetic indices in Paget's disease using dynamic ^{18}F-fluoride positron emission tomography. *J Bone Miner Res.* 2002;17:854–859.
9. Piert M, Zittel TT, Machulla HJ, et al. Blood flow measurements with ^{15}O-H2O and ^{18}F-fluoride ion PET in porcine vertebrae. *J Bone Miner Res.* 1998;13:1328–1336.
10. Messa C, Goodman WG, Hoh CK, et al. Bone metabolic activity measured with positron emission tomography and ^{18}F-fluoride ion in renal osteodystrophy: correlation with bone histomorphometry. *J Clin Endocrinol Metab.* 1993; 77:949–955.
11. Piert M, Zittel TT, Becker GA, et al. Assessment of porcine bone metabolism by dynamic ^{18}F-fluoride ion PET: Correlation with bone histomorphometry. *J Nucl Med.* 2001;42:1091–1100.
12. Brenner W, Vernon C, Muzi M, et al. Comparison of different quantitative approaches to ^{18}F-fluoride PET scans. *J Nucl Med.* 2004;45:1493–1500.
13. Soret M, Bacharach SL, Buvat I. Partial-volume effect in PET tumor imaging. *J Nucl Med.* 2007;48:932–945.
14. Hirata T, Wakita K, Fujioka M, et al. Reliability of one-point blood sampling method for calculating input function in Na^{18}F PET. *Nucl Med Commun.* 2005;26:519–525.
15. Simchowitz L. Interactions of bromide, iodide, and fluoride with the pathways of chloride transport and diffusion in human neutrophils. *J Gen Physiol.* 1988; 91:835–860.
16. Muzi M, Mankoff DA, Grierson JR, Wells JM, Vesselle H, Krohn KA. Kinetic modeling of 3′-deoxy-3′-fluorothymidine in somatic tumors: mathematical studies. *J Nucl Med.* 2005;46:371–380.
17. Mankoff DA, Muzi M, Zaidi H. Quantitative analysis in nuclear oncologic imaging. In: Zaidi H, ed. *Quantitative Analysis in Nuclear Medicine Imaging.* New York, New York: Springer; 2005:494–536.
18. Mankoff DA, Shields AF, Graham MM, Link JM, Eary JF, Krohn KA. Kinetic analysis of 2-(carbon-11)thymidine PET imaging studies: compartmental model and mathematical analysis. *J Nucl Med.* 1998;39:1043–1055.
19. Wells JM, Mankoff DA, Muzi M, et al. Kinetic analysis of 2-(^{11}C)-thymidine PET imaging studies of malignant brain tumors: compartmental model investigation and mathematical analysis. *Mol Imaging.* 2002;1:151–159.
20. Wade AA, Scott JA, Kuter I, Fischman AJ. Flare response in ^{18}F-fluoride ion PET bone scanning. *AJR.* 2006;186:1783–1786.

The Journal of NUCLEAR MEDICINE

Kinetic Analysis of ^{18}F-Fluoride PET Images of Breast Cancer Bone Metastases

Robert K. Doot, Mark Muzi, Lanell M. Peterson, Erin K. Schubert, Julie R. Gralow, Jennifer M. Specht and David A. Mankoff

J Nucl Med. 2010;51:521-527.
Published online: March 17, 2010.
Doi: 10.2967/jnumed.109.070052

The Journal of Nuclear Medicine is published monthly.
SNMMI | Society of Nuclear Medicine and Molecular Imaging
1850 Samuel Morse Drive, Reston, VA 20190.
(Print ISSN: 0161-5505, Online ISSN: 2159-662X)

SNMMI SOCIETY OF NUCLEAR MEDICINE AND MOLECULAR IMAGING